Robust Active Shape Model Based Lung Segmentation in CT Scans

Shanhui Sun[1,2], Christian Bauer[1,2], and Reinhard Beichel[1,2,3]

[1] Dept. of Electrical and Computer Engineering
[2] The Iowa Institute for Biomedical Imaging
[3] Dept. of Internal Medicine
The University of Iowa, Iowa City, IA 52242, USA
reinhard-beichel@uiowa.edu

Abstract. We present a fully automated approach for segmentation of lungs in CT datasets. The method was specifically designed to robustly segment lungs with cancer masses and consists of three processing steps. First, a ribcage detection algorithm is utilized to initialize our model-based segmentation method. Second, a robust active shape model matching approach is applied to roughly segment the outline of the lungs. Third, the outline of the matched model is further adapted to the image data by means of an optimal surface finding approach. The method was evaluated on the LOLA11 test set, consisting of 55 chest CT scans with a variety of different lung diseases and scan protocols. Compared to a reference standard, mean average and median volumetric overlap scores of 0.949 and 0.990 were achieved, respectively. Several examples demonstrate the ability of our method to successfully segment lungs with cancer masses.

1 Introduction

Many automated lung image analysis methods require the segmentation of lungs in an initial processing step. Segmentation of normal lungs imaged with CT is a rather simple task, because of the large density difference between air-filled lung tissue and surrounding tissues. A number of algorithms can be found that deal with this topic (e.g., [1–5]). In case of diseased lungs (e.g., pneumonia, fibrosis, cancer, etc.), lung segmentation becomes a non-trivial problem. Only a few publications propose robust lung segmentation methods [6–10].

To address the limitations of existing methods in the context of segmentation of lungs with cancer masses (robustness, processing speed, etc.), we have introduced a new method [11] which is based on an active shape model (ASM) [12] for lungs in combination with a robust model matching method. The statistical lung model allows us to guide and constrain the segmentation process, and thus, to successfully segment pathological lung tissue which can have similar density to tissue adjacent to the lungs.

The lung segmentation approach utilized in this paper represents an extended version of our work described in [11]. Our method was applied to a diverse test

data set of 55 lung scans, which was provided by the "LObe and Lung Analysis 2011" (LOLA11) challenge[4]. The lung segmentation results achieved with our approach are reported and discussed in this paper.

2 Method

Fig. 1 provides an overview of our approach to lung segmentation, which was designed to robustly segment lungs with cancer masses. The core of our method consists of a robust ASM (RASM) segmentation approach followed by an optimal surface finding (OSF) based segmentation step. Compared to our preliminary work reported in [11], several extensions were incorporated into our algorithm. Specifically, we have added an automated model initialization method, which makes our approach fully automated. Also, the optimal surface finding step was refined by incorporating knowledge about the location of trachea and main bronchi in combination with a more flexible way of generating the basic graph structure required by the OSF algorithm. The individual components of our approach are described below.

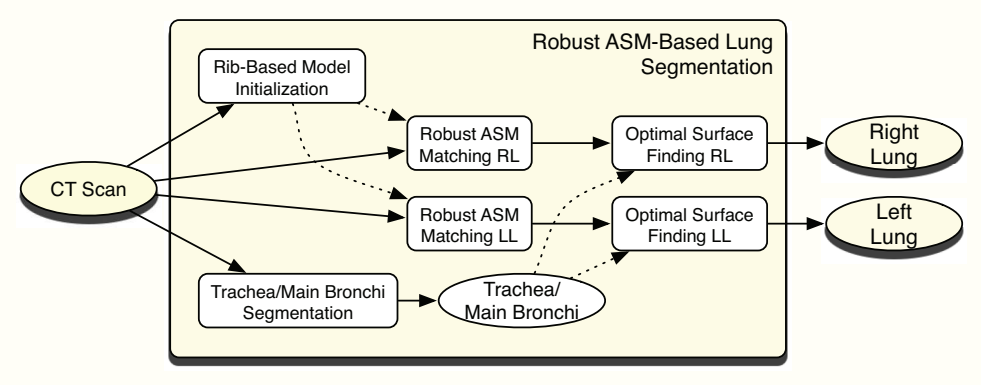

Fig. 1. Method overview. The segmentation of the right lung (RL) and left lung (LL) are performed independently.

2.1 Robust ASM-Based Lung Segmentation

Based on 41 segmented total lung capacity (TLC) CT scans, point distribution models (shape models) of right and left lung shapes were generated. For this task a minimum description length (MDL) approach [13] as described in [11] was utilized. The generated models are then used to segment the right and left

[4] http://www.lola11.com

lung by means of a robust active shape model matching approach, which we have introduced in [11]. The robust matching algorithm allows dealing with outliers which can be induced by high density lung pathology (e.g., cancer) regions. Note that a standard ASM matching approach would fail in such cases, since it is a least squares optimization procedure. Essentially, the methods for model generation and model-based segmentation are the same as described in [11].

2.2 Rib-Based Model Initialization

Before the above described model-based segmentation method can be applied, initial shape and pose parameters need to be found. For this purpose, we utilize the mean shape parameters and calculate location and isotropic scale pose parameters based on a bounding box of the ribcage[5]. Therefore, we utilize an automated method which detects ribs in the CT dataset:

1. To detect tubular structures that are comparable in size, density and scale to rib structures, we truncate the gray-value range of the CT dataset to a range of 0 to 500 HU and apply Frangi's "vesselness measure" [14] on a scale of $\sigma = 5$ mm after downsampling of the dataset by a factor of 4. From the resulting response image, centerline-based representations are extracted utilizing a height-ridge traversal procedure as presented in [15]. This procedure extracts the centerlines of ribs, but the result might also include centerlines of similar structures such as (contrast) enhanced vessels or the spine, for example.
2. In order to discard non-rib like structures, we make use of the observation that the ribs exhibit a repeating pattern, while the other structures do not. For each centerline a feature vector is derived based on geometric properties and mean shift clustering [16] is performed to identify the ribs. We perform a two stage clustering. The features used in the first stage are the eigenvalues resulting from a PCA analysis of the centerline point positions. The resulting clustering allows identification of structures with similar spatial extent as the ribs, but it may still contain some longer blood vessels, for example. Thus, the second clustering stage clusters centerlines based on their orientation, because ribs lie within planes with similar orientation.

2.3 Optimal Surface Finding

Due to the limited size of the training data set utilized for model building, the model might not be able to describe smaller local shape variations. To capture this information, we utilize a constrained optimal surface finding method that is based on the work of Li et al. [17]. The algorithm transforms the segmentation problem into a graph optimization problem represented by a node-weighted directed graph. Therefore, for each surface point of the initial prior surface (the RASM mesh), a search profile is constructed describing possible positions of

[5] Note that we assume that no rotation is required due to the utilized CT protocol.

the mesh vertices with related costs for the surface to pass through this point. Each of these points is represented by a node in the graph with associated costs. Infinite-cost edges between these nodes assure surface smoothness. Li et al. [17] showed how to obtain a globally optimal solution to this segmentation problem in low-order polynomial time using a maximum-flow algorithm [18].

In contrast to our work reported in [11], the search profiles are constructed following vectors in a Gradient Vector Flow [19] field derived from the initial prior surface as described in [20], which allows avoiding mesh folding problems. The required search range (the length of the search profiles) and surface smoothness constraints vary for different locations of the mesh. While in some areas a small search range and restrictive smoothness constraints are preferable to avoid segmentation errors, larger search areas or less restrictive smoothness constraints are necessary in other areas of the prior surface. To address this issue, the search profile length l_v of a vertex v and the smoothness constraints $\Delta_{v1,v2}$ between neighboring vertices are modeled statistically (mean and standard deviation) based on learning data. The actually utilized search profile length l_v of a vertex is obtained as mean plus 2.6 times the standard deviation of these observations; using a value of 2.6 allows including 99% of the found variation. The maximum distance difference $\Delta_{v1,v2}$ between neighboring search profiles is obtained in the same manner. To avoid inclusion of the trachea or the main bronchi in the segmentation results, search profile construction is stopped before entering these regions (see Section 2.4).

As cost function $c(\mathbf{x})$ we use:

$$c(\mathbf{x}) = \begin{cases} 1.0 & if\ \overrightarrow{n}(\mathbf{x}) \cdot \overrightarrow{g}(\mathbf{x}) < 0 \\ 1.0 - |\overrightarrow{g}(\mathbf{x})|/g_{max} & else \end{cases}, \tag{1}$$

where $\overrightarrow{g}(\mathbf{x}) = \nabla(G_\sigma \star I)(\mathbf{x})$ is the image gradient at location $\mathbf{x}$ and g_{max} the highest gradient magnitude in the image I. $\overrightarrow{n}(\mathbf{x})$ is the direction of the search profile at this location and G_σ is a Gaussian filter kernel with variance $\sigma = 2$ mm. The search profile points are obtained at discrete sampling positions with a distance of 0.25 mm between them.

2.4 Trachea and Main Bronchi Segmentation

To avoid leakage of the lung segmentations into the trachea or the main bronchi, we perform a segmentation of these areas and exclude them explicitly from the search space in above described optimal surface finding. Therefore, a modified system of the airway tree extraction method described in [21] is utilized. Because we are only interested in large airways, we reduce the computation time by first downsamping the CT dataset by a factor of 4, before multiscale tube detection filtering is applied for tubular structures with radii 5, 7.5 and 10 mm. Instead of reconstructing the whole airway tree, only the trachea and directly connected tubular structures (the main bronchi) are identified. Accurate segmentations for these structures are obtained by applying a constrained optimal surface finding similar to the method described in the previous section (Section 2.3), but with a fixed search profile length of ± 1 cm and a smoothness parameter of $\Delta = 5$.

3 Results

We applied our method to the LOLA11 test set. For performance assessment, all lung meshes generated with our approach were voxelized and sent to the LOLA11 organizers, which in return provided the volumetric segmentation overlap measures with respect to a ground truth[6]. In Table 1, the results for left and right lungs are shown which consist of the mean, standard deviation, minimum, first quartile, median, third quartile, and maximum overlap of the 55 test cases, as well as an overall score. In this context, the overlap between two binary segmentation volumes is defined as the volume of their intersection divided by the volume of their union.

Table 1. Results of lung segmentation for the 55 scans on LOLA11.

	mean	SD	min	Q1	median	Q3	max
left lung	0.939	0.173	0.0392	0.979	0.990	0.994	0.997
right lung	0.959	0.122	0.167	0.985	0.990	0.994	0.998
score	0.949						

On average, about 6 minutes were required for fully automated segmentation of right and left lungs in a CT scan.

4 Discussion

Left and right lung segmentations show the same median overlap value of 0.990 (Table 1), which is an indication that in the majority of results generated with our approach closely match the gold standard produced by the organizers of LOLA11. The examples depicted in Figs. 2, 3, and 4 confirm this—segmentations of normal lungs and lungs with high-density pathology (e.g., lung cancer) show only small errors.

As can be seen from Table 1, the mean overlap value for segmented left and right lungs is below the median and first quartile (Q1). This indicates that our approach failed in a few cases. This is also reflected by the minimum overlap values shown in Table 1. Figs. 5 and 6 depict some examples of segmentation errors. In cases where the lung shape widely deviates from the learned lung shapes (Fig. 5)—e.g. collapsed or partly removed lungs—model-based segmentation is challenging. For some CT scans (e.g., with pleural effusion), additional post-processing steps might be needed to extract the actual lung tissue.

The lung imaged in Fig. 6(a) appears to be quite long. Since our model-based approach is constrained to a certain degree by the learned lung shapes, it fails to fully segment this case. Such a problem can be solved by expanding the learning shape set. Fig. 6(b) depicts a case where the tips of the left and right lungs

[6] Details regarding the validation procedure can be found at http://www.lola11.com

overlapped. This problem can be solved by utilizing a multiple surface graph search approach as described in [17].

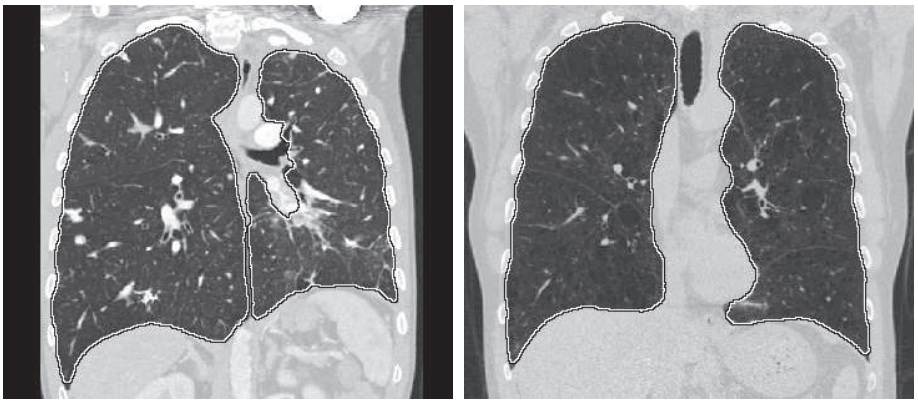

(a) (b)

Fig. 2. Examples of lung segmentations in CT images with (a) and without (b) contrast agent.

5 Conclusion and Future Work

We have presented a fully automated method for the segmentation of volumetric CT scans of lungs with high density pathology. Our approach is based on a robust ASM matching method which is followed by a constrained optimal surface finding step. The evaluation on the LOLA11 test set showed that the majority of lung segmentations produced with our approach has a high volumetric overlap with the gold standard. Larger segmentation errors occurred in cases with wide deviations from the shapes in the utilized learning set. Future work will focus on expanding the learning set utilized for model generation and on refining the optimal surface finding step of our method.

Acknowledgments

This work was supported in part by the Biological Sciences Funding Program of The University of Iowa and by NIH/NIBIB grant 5R01EB004640-05. The authors thank Dr. Eric A. Hoffman and Dr. Joseph M. Reinhardt at the University of Iowa for providing lung data sets.

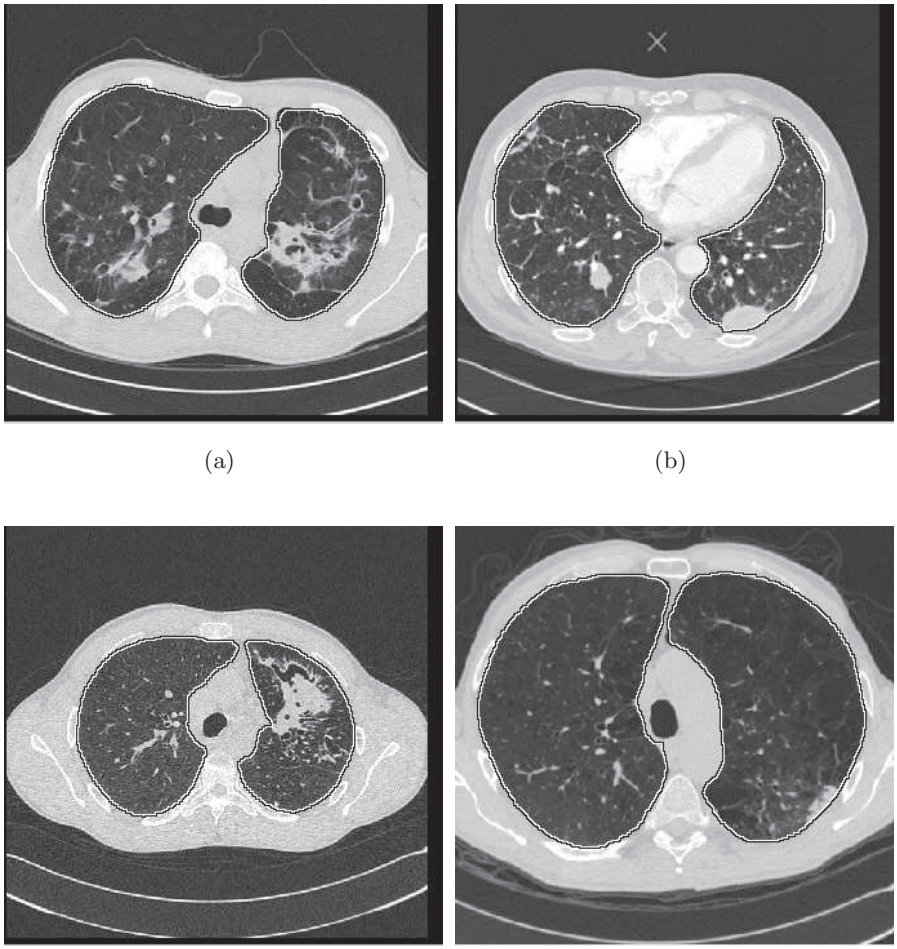

(a) (b)

(c) (d)

Fig. 3. Examples of lung segmentations. The axial images depict lungs with different types of high density pathology.

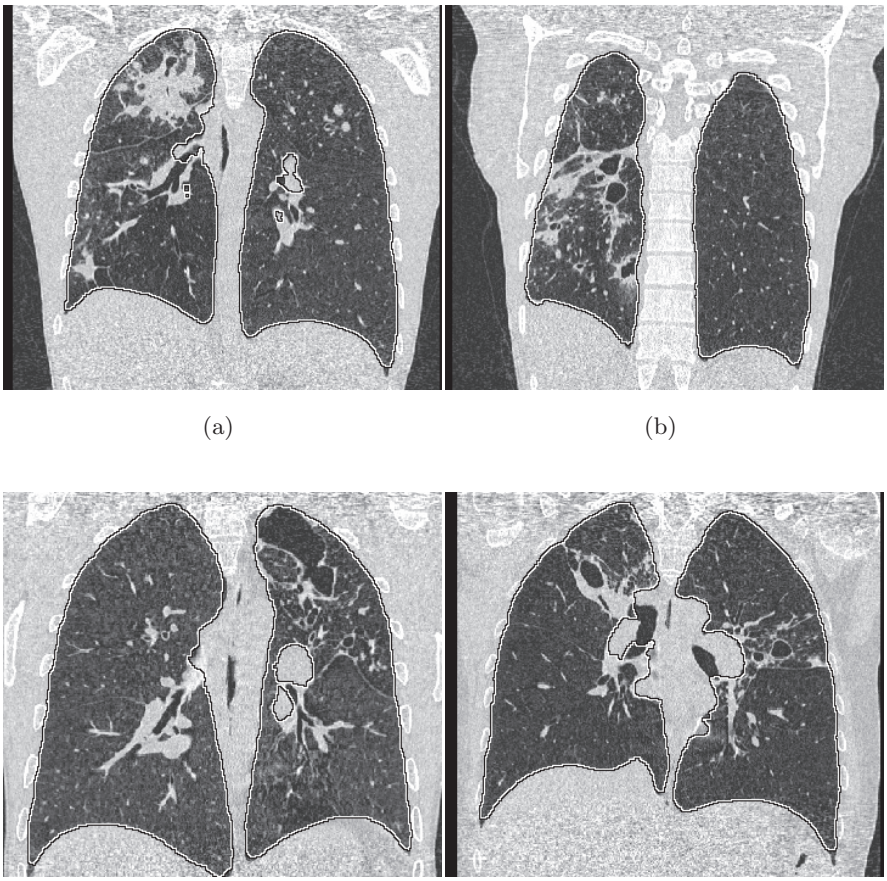

(a) (b)

(c) (d)

Fig. 4. Examples of lung segmentations showing coronal views of lungs with high density pathology.

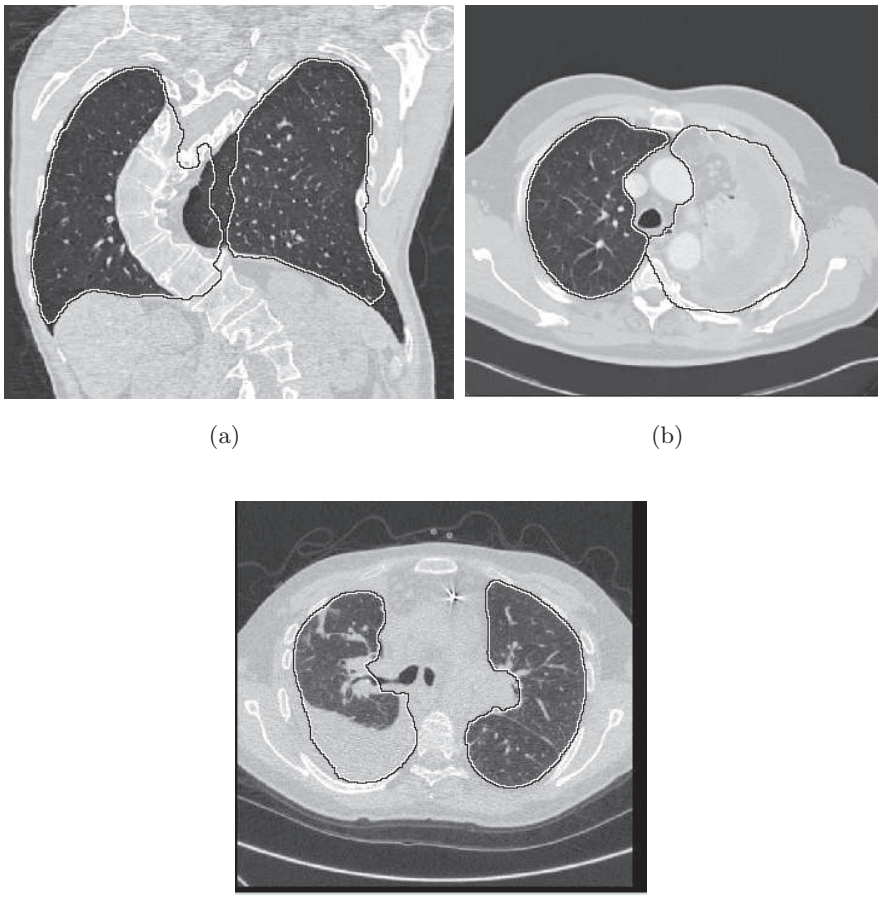

(a) (b)

(c)

Fig. 5. Examples of lung shape variation in the LOLA11 test set. For each CT scan, the corresponding segmentation results is depicted.

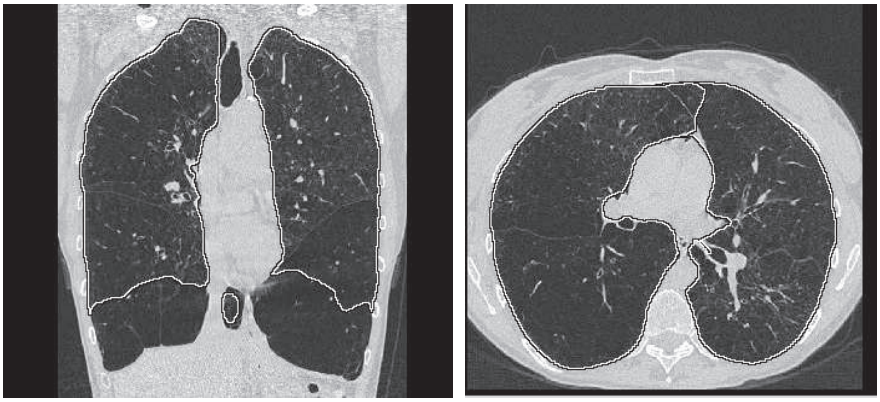

(a) (b)

Fig. 6. Examples of current limitations of our segmentation approach. See Section 4 for details.

References

1. Armato, S.G., Sensakovic, W.F.: Automated lung segmentation for thoracic CT. Acad. Radiol. **11**(9) (2004) 1011–1021
2. Leader, J.K., Zheng, B., Rogers, R.M., Sciurba, F.C., Perez, A., Chapman, B.E., Patel, S., Fuhrman, C.R., Gur, D.: Automated lung segmentation in X-ray computed tomography. Acad. Radiol. **10**(11) (2003) 1224–1236
3. Silva, A., Silva, J.S., Santos, B.S., Ferreira, C.: Fast pulmonary contour extraction in X-ray CT images: a methodology and quality assessment. In: Proc. SPIE (Medical Imaging). Volume 4321. (2001) 216–224
4. Hu, S., Hoffman, E.A., Reinhardt, J.M.: Automatic lung segmentation for accurate quantitation of volumetric X-ray CT image. IEEE Trans. Med. Imag. **20**(6) (2001) 490–498
5. Hoffman, E.A., Sinak, L.J., Robb, R.A., Ritman, E.L.: Noninvasive quantitative imaging of shape and volume of lungs. Journal of Applied Physiology **54**(5) (1983) 1414–1421
6. Sluimer, I., Prokop, M., van Ginneken, B.: Toward automated segmentation of the pathological lung in CT. IEEE Trans. Med. Imag. **24**(8) (2005) 1025–1038
7. Pu, J., Roos, J., Yi, C.A., Napel, S., Rubin, G.D., Paik, D.S.: Adaptive border marching algorithm: Automatic lung segmentation on chest CT images. Computerized Medical Imaging and Graphics **32**(6) (2008) 452 – 462
8. Prasad, M.N., Brown, M.S., Ahmad, S., Abtin, F., Allen, J., da Costa, I., Kim, H.J., McNitt-Gray, M.F., Goldin, J.G.: Automatic segmentation of lung parenchyma in the presence of diseases based on curvature of ribs. Academic Radiology **15**(9) (2008) 1173 – 1180
9. Wang, J., Li, Q., Li, F.: Automated segmentation of lungs with severe interstitial lung disease in CT. Medical Physics **36**(10) (2009) 4592 – 4599

10. van Rikxoort, E.M., de Hoop, B., Viergever, M.A., Prokop, M., van Ginneken, B.: Automatic lung segmentation from thoracic computed tomography scans using a hybrid approach with error detection. Medical Physics **36** (2009) 2934–2947
11. Sun, S., McLennan, G., Hoffman, E.A., Beichel, R.: Model-based segmentation of pathological lungs in volumetric CT data. In: Proc. of Third International Workshop on Pulmonary Image Analysis. (2010) 967–974
12. Cootes, T.F., Cooper, D., Taylor, C.J., Graham, J.: Active shape models - their training and application. Computer Vision and Image Understanding **61**(1) (1995) 38–59
13. Heimann, T., Wolf, I., Williams, T., Meinzer, H.P.: 3D active shape models using gradient descent optimization of description length. In: In Proc. IPMI. Volume 3565., Springer, Heidelberg (2005) 566–577
14. Frangi, A.F., Niessen, W.J., Vincken, K.L., Viergever, M.A.: Multiscale vessel enhancement filtering. In: LNCS. Volume 1496., MICCAI (1998) 130–137
15. Bauer, C., Pock, T., Sorantin, E., Bischof, H., Beichel, R.: Segmentation of interwoven 3D tubular tree structures utilizing shape priors and graph cuts. Medical Image Analysis **14** (2010) 172–184
16. Cheng, Y.: Mean shift, mode seeking, and clustering. Pattern Analysis and Machine Intelligence **17**(8) (August 1995) 790–799
17. Li, K., Wu, X., Chen, D., Sonka, M.: Optimal surface segmentation in volumetric images - a graph-theoretic approach. IEEE Trans. Pattern Anal. Machine Intell. **28**(1) (2006) 119–134
18. Boykov, Y., Kolmogorov, V.: An experimental comparison of Min-Cut/Max-Flow algorithms for energy minimization in vision. IEEE Transactions on Pattern Analysis and Machine Intelligence **26** (September 2004) 1124–1137 ACM ID: 1018355.
19. Xu, C., Prince, J.L.: Snakes, shapes, and gradient vector flow. Image Processing, IEEE Transactions on **7**(3) (March 1998) 359–369
20. Bauer, C., Sun, S., Beichel, R.: Avoiding mesh folding in 3D optimal surface segmentation. In: 7th International Symposium on Visual Computing (to appear). (2011)
21. Bauer, C., Pock, T., Bischof, H., Beichel, R.: Airway tree reconstruction based on tube detection. In: Proc. of Second International Workshop on Pulmonary Image Analysis. (2009) 203–213